Atmos. Chem. Phys. Discuss., 12, 30259–30282, 2012
www.atmos-chem-phys-discuss.net/12/30259/2012/
doi:10.5194/acpd-12-30259-2012

Atmospheric Chemistry and Physics Discussions

An analysis of atmospheric CH_4 concentrations from 1984 to 2008 with a single box atmospheric chemistry model

Z. Tan[1] **and Q. Zhuang**[1,2]

[1]Department of Earth, Atmospheric and Planetary Sciences, Purdue University, West Lafayette, IN, USA
[2]Department of Agronomy, Purdue University, West Lafayette, IN, USA

Received: 17 July 2012 – Accepted: 5 November 2012 – Published: 22 November 2012

Correspondence to: Z. Tan (tan80@purdue.edu)

Published by Copernicus Publications on behalf of the European Geosciences Union.

Abstract

We present a single box atmospheric chemistry model involving atmospheric methane (CH_4), carbon monoxide (CO) and radical hydroxyl (OH) to analyze atmospheric CH_4 concentrations from 1984 to 2008. When OH is allowed to vary, the modeled CH_4 is 20 ppb higher than observations from the NOAA/ESRL and AGAGE networks for the end of 2008. However, when the OH concentration is held constant at 10^6 molecule cm^{-3}, the simulated CH_4 shows a trend approximately equal to observations. Both simulations show a clear slowdown in the CH_4 growth rate during recent decades, from about 13 ppb yr^{-1} in 1984 to less than 5 ppb yr^{-1} in 2003. Furthermore, if the constant OH assumption is credible, we think that this slowdown is mainly due to a pause in the growth of wetland methane emissions. In simulations run for the Northern and Southern Hemispheres separately, we find that the Northern Hemisphere is more sensitive to wetland emissions, whereas the southern tends to be more perturbed by CH_4 transportation, dramatic OH change, and biomass burning. When measured CO values from NOAA/ESRL are used to drive the model, changes in the CH_4 growth rate become more consistent with observations, but the long-term increase in CH_4 is underestimated. This shows that CO is a good indicator of short-term variations in oxidizing power in the atmosphere. The simulation results also indicate the significant drop in OH concentrations in 1998 (about 5 % lower than the previous year) was probably due to an abrupt increase in wetland methane emissions during an intense El Niño event. Using a fixed-lag Kalman smoother, we estimate the mean wetland methane flux is about 128 Tg yr^{-1} through the period 1984–2008. This study demonstrates the effectiveness in examining the role of OH and CO in affecting CH_4.

1 Introduction

Atmospheric methane (CH_4) is of considerable interest due to its importance as the second most powerful greenhouse gas, and the significant role it plays in ozone layer

ACPD
12, 30259–30282, 2012

chemistry (Forster et al., 2007; Denman et al., 2007). The global atmospheric methane burden has more than doubled since pre-industrial times (Etheridge et al., 1992), raising concerns that it is contributing to global warming and will continue to do so in the future. However, although these past increases were alarmingly rapid, trends for the period from 1984 to 2008 show a surprisingly persistent slowdown, reaching nearly zero in the 1990s with renewed growth at the start of 2007 (Steele et al., 1992; Dlugokencky et al., 1998, 2003; Rigby et al., 2008). These unexpected changes in atmospheric CH_4 abundance imply that there are still large uncertainties in our understanding of how the imbalance between CH_4 sources and sinks is changing with time and the underlying reasons. For example, methane is destroyed as a result of reaction with the hydroxyl radical (OH) (Fung et al., 1991), predominantly in the troposphere, but as the chemical mechanism of the hydroxyl radical's formation and destruction in the troposphere is still under investigation (Taraborrelli et al., 2012), the assessment of the [OH] trend varies in different studies, giving rise to large uncertainties (Prinn et al., 2001, 2005; Bergamaschi et al., 2000). Additionally, as the largest natural source of methane, emissions from wetlands are very sensitive to environmental factors including input of organic carbon, carbon substrate type, temperature, and soil water table level (Zhuang et al., 2004), which leads to concerns of positive climate-CH_4 feedbacks (Ringeval et al., 2011). To explore the possible reasons for atmospheric methane changes during the last several decades, we develop a single-box atmospheric chemistry model involving CH_4, CO and OH and apply this model for the period 1984–2008. Based on this model, we use an atmospheric inversion method, the fixed-lag Kalman smoother (Hartley and Prinn et al., 1993; Bruhwiler et al., 2005), to estimate wetland methane emissions for the same time period.

ACPD
12, 30259–30282, 2012

2 Method

2.1 A single box atmospheric chemistry model

Four types of processes control the concentrations of chemical species in the atmosphere: emissions, chemistry, transportation and deposition. A general mathematical approach to describe how the above processes determine the atmospheric concentrations of species is given in the form of the continuity equation. When only the global mean concentration is concerned, a single box atmospheric chemistry model without transport is a practical way to approximate the real atmospheric system. Instead of considering CH_4 alone, we also include CO and OH in the model, as earlier studies indicated strong interactions exist among these three species, which can be expressed by two important reactions (Thompson et al., 1986):

$$CH_4 + OH \rightarrow CH_3 + H_2O \quad \text{(R1)}$$

$$CO + OH \xrightarrow{O_2} CO_2 + HO_2 \quad \text{(R2)}$$

Reaction (R1) represents methane's oxidation by hydroxyl radicals, which is its predominant sink in the atmosphere. It is also responsible for the production of a considerable amount of atmospheric CO. Reaction (R2) represents the dominant destruction pathway for both atmospheric CO and OH.

Overall, we include all primary emission, chemistry and deposition processes of CH_4, CO and OH in this single box model, and express them in the following continuity equations:

$$\frac{d[CH_4]}{dt} = A_w Q_{10}^{0.1\times(T-T_{mean})} + S_{CH_4} - k_{CH_4+OH}[CH_4][OH] - L_{CH_4} \quad (1)$$

$$\frac{d[CO]}{dt} = S_{CO} + k_{CH_4+OH}[CH_4][OH] - k_{CO+OH}[CO][OH] - L_{CO} \quad (2)$$

ACPD
12, 30259–30282, 2012

$$\frac{d[OH]}{dt} = S_{OH} - k_{CH_4+OH}[CH_4][OH] - k_{CO+OH}[CO][OH] - k_{X+OH}[OH] \quad (3)$$

where the first item on the right side of Eq. (1) is a Q_{10} function accounting for the temperature dependence of wetland methane emissions (A_w is a wetland area coefficient, $Q_{10} = 6.0$ and $T_{mean} = 14\,^{\circ}C$) (Walter et al., 2000). S_{CH_4} is the total methane emissions, minus the emissions from wetlands; this includes fossil fuel sources, rice production, landfills, ruminant animals and biomass burning ($\sim 385\,Tg\,yr^{-1}$) (Fung et al., 1991). k_{CH_4+OH} is the rate constant of Reaction (R1), and L_{CH_4} is methane surface deposition by soil uptake ($\sim 10\,Tg\,yr^{-1}$) (Fung et al., 1991). In Eq. (2), S_{CO} represents all CO sources except CH_4 oxidation, which includes VOC oxidation and emissions from vegetables, oceans, fossil fuel combustion and biomass burning, k_{CO+OH} is the rate constant of Reaction (R2), and L_{CO} is surface deposition of carbon monoxide ($\sim 290\,Tg\,yr^{-1}$) (Bergamaschi et al., 2000). In Eq. (3), as isoprene oxidation has been suggested to serve as both a sink and source for hydroxyl radicals (Taraborrelli et al., 2012), it is necessary to also include OH production from this pathway into OH sources, S_{OH} (the majority of OH is still produced by photolysis of O_3). $k_{X+OH}[OH]$ accounts for all OH chemical losses independent from CH_4, CO oxidations. In other aspects, L_{CH_4} and L_{CO} are assumed to be proportional to CH_4 and CO concentrations, respectively. Because our interest lies in the impact of global warming on atmospheric CH_4 concentrations, and only wetland methane fluxes show clear evidence of sensitivity to climate change, S_{CH_4} and S_{CO} are held constant in the model.

Many studies have indicated that the anomalies in CH_4 concentrations don't always occur simultaneously and with equal intensity in the Northern and Southern Hemispheres (Dlugokencky et al., 1994; Prinn et al., 2005; Rigby et al., 2008). For this reason, it is necessary to simulate methane concentrations separately in the two hemispheres to order to investigate the origins of these anomalies. Although our model contains only one box, by adding a constant southward transportation item to Eq. (1), it is still feasible for this model to study the changes of atmospheric CH_4, CO and OH in

ACPD
12, 30259–30282, 2012

Northern and Southern Hemispheres. Table 1 shows the distributions of sources and sinks of CH_4, CO and OH on the earth used in our model (Bergamaschi et al., 2000; Fung et al., 1991).

2.2 Data and simulation protocol

To analyze CH_4 concentrations in recent decades, we run the single box atmospheric chemistry model from 1984 to 2008. In addition to the initial concentrations of CH_4, CO and OH, as wetland emissions are a function of temperature in Eq. (1), land surface temperature data is also an indispensable input for model simulation. Our model uses monthly mean land surface temperature calculated from a global, 50-yr, 3-hourly, 1.0° dataset of meteorological forcing, Global Meteorological Forcing Dataset for Land Surface Modeling (Seinfeld et al., 2006). This dataset is constructed by combining a suite of global observation-based datasets with the National Centers for Environmental Prediction-National Center for Atmospheric Research (NCEP-NCAR) reanalysis, available from 1948 to 2008 (Seinfeld et al., 2006). To address the seasonal differences between the two hemispheres, we calculate methane fluxes from the Northern and Southern Hemisphere separately and then sum them up together.

For the purpose of model assessment, we also present global mean atmospheric CH_4 and CO concentrations derived from GLOBALVIEW 2009 data and measurements of the global monitoring network operated by Advanced Global Atmospheric Gases Experiment (AGAGE). GLOBALVIEW-CH4 and GLOBALVIEW-CO products are derived from measurements of the cooperative flask sampling network operated by Global Monitoring Division of NOAA's Earth System Research Laboratory (ESRL) using the data extension and data integration techniques (GLOBALVIEW-CH4, 2009; GLOBALVIEW-CO, 2009). The NOAA/ESRL network consists of 54 fixed sites sampled roughly weekly, and shipboard sites collected roughly every 3 weeks, distributed from the South Pole to Greenland (Dlugokencky et al., 2009). GLOBALVIEW data is dominated by samples representative of the marine boundary layer at remote locations from known or suspected methane source regions. The AGAGE network consists of five

ACPD
12, 30259–30282, 2012

stations located in coastal regions, equally distributed from 53° N to 41° S (Mace Head, Ireland; Trinidad Head, California; Ragged Point, Barbados; Cape Matatula, American Samoa; Cape Grim, Tasmania) (http://agage.eas.gatech.edu/data_archive/; STANDARD AGAGE REF.; Prinn et al., 2000), which measure high-precision, high-frequency air samples (approximately every 40 min). Currently the NOAA/ESRL measurements are available from 1984 to 2009, and the AGAGE measurements are available from 1997 to 2009.

2.3 The inversion problem and its lagged-form

Unlike process-based biogeochemistry models, atmospheric inversion is a method to estimate trace gas surface fluxes by using concentration observations as constraints. The inversion problem can be characterized by the solution of

$$z = \mathbf{H}s + v \tag{4}$$

where z is a vector of observations, s is a state vector, including emissions and depositions, $\mathbf{H}$ is the measurement sensitivity matrix, and v is the uncertainty of the approximated observations $\mathbf{H}s$ with respect to the real observation z. Assuming uncertainties in the observations and state vector are both Gaussian, Eq. (4) can be treated as a linear quadratic estimation problem (LQE). LQE problems can be solved in the "batch" mode (Gelb, 1974) that treats all observations simultaneously. But this approach is cumbersome to implement when more observations become available. Instead, the fixed-lag Kalman smoother (KS) is widely used, because of the ease of implementation and its efficiency when assimilating observations sequentially (Hartley and Prinn et al., 1993).

The fixed-lag KS was developed based on the fact that a certain flux will be fully blended into the background after a sufficient time of transport, such that the observations at a particular time step can only significantly constrain fluxes that occur within a short timeframe right before the given step (Bruhwiler et al., 2005). For this reason, state variables are accordingly divided into two groups: on-line state variables (fluxes

ACPD
12, 30259–30282, 2012

that are still under optimization) and off-line state variables (fluxes that are no longer updated). The lagged form of Eq. (4) for KS is

$$z_J = \begin{bmatrix} \mathbf{H}_{J,J} & \mathbf{H}_{J,J-1} & \cdots & \mathbf{H}_{J,J-P+1} & \mathbf{H}_{J,J-P} & \cdots & \mathbf{H}_{J,1} \end{bmatrix} \begin{bmatrix} s_J \\ s_{J-1} \\ \vdots \\ s_{J-P+1} \\ s_{J-P} \\ \vdots \\ s_1 \end{bmatrix} \tag{5}$$

$$= \begin{bmatrix} \mathbf{H}_u & \mathbf{H}_v \end{bmatrix} \begin{bmatrix} s_u \\ s_v \end{bmatrix}$$

where z_J is the observation at time J, s_u is the vector of on-line state variables from time J back to time $J-P+1$, and s_v is the vector of off-line state variables, from time $J-P$ back to initial time. P is the number of months of fluxes that are still under optimization at each time step, which also means that each month of flux is estimated using P months of subsequent observations. In this study, we assume global methane concentration at time J can be used to update the six-month fluxes from J to $J-5$ ($P=6$) (Bruhwiler et al., 2005). Observation matrix $\mathbf{H}_u$ and $\mathbf{H}_v$ can be calculated from Greenfunction formalism of Eq. (1) (Enting, 2002).

In the fixed-lag Kalman smoother, on-line fluxes and their covariance are updated sequentially by Eqs. (6) and (7) (Hartley and Prinn et al., 1993),

$$s_u^+ = s_u^- + K_u(z_J - \mathbf{H}_u s_u^- - \mathbf{H}_v s_v^+) \tag{6}$$

$$Q_u^+ = Q_u^- - K_u \mathbf{H}_u^{\mathrm{T}} Q_u^- \tag{7}$$

where superscript $-$ indicates the prior estimation, and $+$ indicates posterior inference. K_u is Kalman gain, defined in Eq. (8),

$$K_u = Q_u^- \mathbf{H}_u^{\mathrm{T}} (R + \mathbf{H}_u^{\mathrm{T}} Q_u^- \mathbf{H}_u^{\mathrm{T}})^{-1} \tag{8}$$

ACPD
12, 30259–30282, 2012

where R is the observation error variance at time J. This value can be calculated from standard deviation data of methane measurements in the NOAA/ESRL dataset As shown in Eqs. (6) and (7), in each time step J, the fixed-lag KS will update the estimation of the latest six-month fluxes (index from J to $J-5$) and their covariance, using global monthly methane concentration at time J (z_J) and prior information of these six on-line state variables (s_u^- and Q_u^-). As Eq. (5) implies, in the time step J, except for the newest flux (s_J), the older five fluxes and their covariance have been updated in the estimation process for at least one time. So their mean and covariance can be set as equal to the posterior values estimated from Eqs. (6) and (7) in the time step $J-1$. But for the flux at time J, as it is totally new for the estimation process, its prior information is initialized in the following way: first, we set the prior mean and variance for this flux as $150\,\mathrm{Tg\,yr^{-1}}$ and $50\,\mathrm{Tg\,yr^{-1}}$, respectively, according to Fung's estimation (Fung et al., 1991), which list the range of wetland methane flux from 100 to $200\,\mathrm{Tg\,yr^{-1}}$. Then, for the correlations between this flux and fluxes from $J-1$ to $J-5$, they are calculated by analyzing the time series of the Q_{10} function in Eq. (1).

From Eq. (1), we can see that the levels of atmospheric OH concentration can determine the amount of chemical losses of CH_4 in the atmosphere and thus also determine the estimate amount of methane emissions. Currently there are two competing assumptions for OH changes: one assumption reckons that atmospheric OH remains nearly constant in the long term, and the other assumption recognizes that atmospheric OH should decrease with the growth of CO and CH_4 (Manning et al., 2005; Thompson et al., 1986). In this work, we utilize the fixed-lag KS to estimate wetland methane fluxes for both assumptions. In the first experiment, OH is fixed at $10^6\,\mathrm{molecule\,cm^{-3}}$, and in the second, OH concentrations from 1984 to 2005 are referred to Prinn's publication (Prinn et al., 2005). Other methane emissions, except for wetland fluxes, are set to total about $385\,\mathrm{Tg\,yr^{-1}}$, and soil uptake is set at about $10\,\mathrm{Tg\,yr^{-1}}$.

ACPD
12, 30259–30282, 2012

3 Results and discussion

3.1 Comparison of model simulations and atmospheric observations

Figure 1a–c show the difference between observed and simulated values of global monthly methane concentration (ppb) and the global methane growth rate (ppb yr^{-1}) from 1984 to 2008. At first our simulation reveals a clear slowdown in the methane growth rate during this period that also has been suggested by other studies (Dlugokencky et al., 1998, 2003). Because the concentrations of hydroxyl radical decline from 10 to 9.76×10^5 molecule cm^{-3} in the experiment, this slowdown is more likely a result of the stabilization of methane emissions, which was caused either by weakened global warming or by constrained anthropogenic emissions. Our simulation also implies that climate change is responsible for at least one methane concentration anomaly in recent decades: the abrupt global methane increase during the El Niño events of 1997 and 1998 (Dlugokencky et al., 2001). However, Fig. 1a, c also indicate that our model underestimates the variations in the methane growth rate and overestimates methane increase in the 21st century. From 2000 onward, the modeled CH_4 concentrations lay above observed values, with modeled CH_4 eventually reaching 20 ppb higher than observed values at the end of 2008. We think one possible reason for this bias is that the methane emissions from non-wetland sources, such as the natural gas industry, decreased beginning in 2000. However, we lack emission data to validate this hypothesis. Another possible explanation is that, unlike the continuous decline seen in the model, the concentration of atmospheric OH has remained nearly constant in recent decades (Manning et al., 2005; Prinn et al., 2005), which would mean that there should have been more CH_4 destructed by OH oxidation in the atmosphere than was simulated. Furthermore, if atmospheric OH declines with time, CO abundance should increase accordingly for the attenuation of oxidation power, as in our model, where the simulated CO rose from 93 to 96.9 ppb. However, measurements from NOAA/ESRL show that atmospheric CO is even slightly lower in 2000s than in 1990s.

ACPD
12, 30259–30282, 2012

Figure 2a–c show the difference between observations and model-simulated values of monthly methane concentration (ppb) and methane growth rate (ppb yr^{-1}) in the Northern Hemisphere from 1984 to 2008, and Fig. 3a–c show the difference in the Southern Hemisphere during the same period. Once again, simulations show clear slowdowns in the methane growth rate in both hemispheres. However, the difference is much less in the Southern Hemisphere than in the Northern Hemisphere (at the end of 2008, modeled CH_4 is 40 ppb higher than observations in the Northern Hemisphere, but nearly at the same level of observations in the Southern Hemisphere). This bias suggests that the factors, which reduce CH_4 concentrations in the atmosphere, mainly originate from the Northern Hemisphere, on the condition that OH really has decreased in recent decades. Figure 2c shows a clear growth of methane concentrations in 2007 and 2008, but Fig. 3c does not; we think the observed renewed rise in global methane concentrations was caused by a wetland methane emission increase strongly biased to the Northern Hemisphere (Rigby et al., 2008). In the model, simulated [CO] increases from 120 to 125.2 ppb in the north and from 66 to 68.6 ppb in the south, and meanwhile simulated [OH] decreases from 10 to 9.73×10^5 molecule cm^{-3} in the north and from 10 to 9.8×10^5 molecule cm^{-3} in the south.

3.2 Roles of OH and CO in CH_4 changes

In Sect. 3.1, we suggest that atmospheric OH may be stable over a long time scale. To examine this hypothesis, we deactivate Eq. (3) in our model and conduct a simulation with OH concentration fixed at 10^6 molecule cm^{-3}. Figure 1d–f show the difference between observations and model-simulated values of global monthly methane concentration (ppb) and the global methane growth rate (ppb yr^{-1}) for this scenario. In Fig. 1d, the simulated CH_4 concentrations vary in a manner consistent with measurements, both before and after 2000. Figure 1f also shows that methane growth rate decreases more rapidly than it does in the changing OH scenario. All these improvements seemingly could support the argument that there is no significant long-term trend in hydroxyl radical concentrations but recurring short-term variations of around ten percent persist-

ACPD
12, 30259–30282, 2012

ing for a few months (Manning et al., 2005). Furthermore the short-term variations are probably produced by sources and sinks that are not well presented in our model, e.g. changes in tropical tropospheric UV flux after the eruption of Mt. Pinatubo in 1991 (Dlugokencky et al., 1996), and biomass burning by large boreal wildfires in 2002 and 2003 (Prinn et al., 2005). In this simulation, atmospheric CO increases from 93 to 95.6 ppb.

We also ran our model under the constant OH assumption in the Northern and Southern Hemispheres, respectively. Figure 2d–f show the comparison between observations and model simulations in the north, and Fig. 3d–f show it in the South. Compared to the changing OH cases, the simulations here behave very differently; the modeled methane concentrations get closer to measurements in the Northern Hemisphere, but depart more from the measurements in the Southern Hemisphere. We think this distinction can be explained by the different properties of two hemispheres. As the Northern Hemisphere is covered by a large amount of lands, wetland and rice agriculture emissions (both sensitive to climate change) can dominate the trend of atmospheric methane. But this is not the case in the Southern Hemisphere. In the South, as its most areas are covered by oceans, these climate-sensitive emissions are too small to control methane changes. In contrast, methane concentrations there are easily influenced by transportations, abrupt OH changes and biomass burning, which, as described in Sect. 2.1, have been set to constant in our model for simplicity. In the simulations, modeled [CO] increases from 120 to 122.9 ppb in the north and from 66 to 68 ppb in the south.

Figure 4a–d show global monthly methane concentration (ppb), methane growth rate (ppb yr^{-1}), and the trajectory of atmospheric OH when using CO concentrations from NOAA/ESRL as another input of model. We find the simulated [CH_4] is 20 ppb lower than observations in most periods (shown in Fig. 4a), but the changes in the methane growth rate agree with observations considerably (shown in Fig. 4d). In this scenario, as CO abundance from the NOAA/ESRL dataset decreases in the observation period, not considering the buffer effect of VOC oxidation, OH concentrations should increase correspondingly; this, in turn could reduce atmospheric CH_4 by oxidation. But according

ACPD
12, 30259–30282, 2012

to the claims of other studies, atmospheric OH is either unchanged or decreased with time (Prinn et al., 2005; Bousquet et al., 2005). So we guess that a mechanism to stabilize OH concentrations should exist, and the lack of formulation of this mechanism in our model has caused the discrepancy in Fig. 4a. Meanwhile, as the short-term variations of OH are still largely controlled by CO changes (Manning et al., 2005), the adoption of real CO data improves the agreement of CH_4 growth rate in Fig. 4d. Figure 4b shows the changes in oxidizing power (OH concentrations) in the atmosphere from 1991 to 2008, in which an abrupt decrease of OH concentrations in 1997 and 1998 was caused by an intense El Niño event (Prinn et al., 2005).

3.3 Wetland emissions

Figure 5 shows the estimations of wetland methane fluxes using the fixed-lag Kalman smoother based on two different assumptions described in Sect. 2.3. Overall our estimations are close to Khalil's (Khalil et al., 2007), and the average flux estimated is about 128 $Tg\,yr^{-1}$ from 1984 to 2008 (Khalil's estimation is about 125 $Tg\,yr^{-1}$). As expected, the changing OH case demonstrates more dramatic changes in wetland emissions than the constant OH case. Several apparent peaks of estimated wetland fluxes occur in 1991, 1998 and 2008. Because other methane sources besides wetland emissions are set as constant, changes in methane fluxes in other ways would be also attributed to wetland incorrectly, for example, the peak in 1991 should be attributed to the eruption of Mt. Pinatubo.

4 Conclusions

Using a simple one-box atmospheric chemistry model involving CH_4, CO and OH, we can more efficiently re-construct atmospheric methane concentration trajectory in recent decades in comparison with using 3-D transport and chemistry models (Patra et al., 2011) Our simulation indicates if atmospheric OH is varying, besides wetland

ACPD
12, 30259–30282, 2012

fluxes and chemical losses, there should be other sources or sinks that can influence methane concentrations significantly, but if OH is constant during our simulation period, atmospheric CH_4 can be predominantly determined by these two factors. Therefore it is impossible to predict the future methane changes without understanding OH trends. In addition, hemispheric simulations show that methane concentrations in the Northern Hemisphere are largely controlled by wetland fluxes, and thus are more sensitive to climate change. The simulation using measured CO concentrations underestimates CH_4 growth in recent decades, but gives a better description of methane growth rate variations. Meanwhile the model shows a dramatic decrease of OH concentrations in 1998, which might be linked with an intense El Niño event. With the fixed-lag Kalman smoother, we estimate the global wetland methane emissions to be approximately $128\,\mathrm{Tg\,yr^{-1}}$.

Acknowledgements. We acknowledge the Earth System Research Laboratory of NOAA and Advanced Global Atmospheric Gases Experiment, who provide their atmospheric CH_4 mixing ratio data. The land surface temperature data for this study are from the Research Data Archive (RDA) which is maintained by the Computational and Information Systems Laboratory (CISL) at the National Center for Atmospheric Research (NCAR). NCAR is sponsored by the National Science Foundation (NSF). The original data are available from the RDA (http://rda.ucar.edu) in dataset number ds314.0.

References

Bergamaschi, P., Hein, R., Heimann, M., and Crutzen, P. J.: Inverse modeling of the global CO cycle 1. Inversion of CO mixing ratios, J. Geophy. Res., 105, 1909–1927, doi:10.1029/1999JD900818, 2000.

Bousquet, P., Hauglustaine, D. A., Peylin, P., Carouge, C., and Ciais, P.: Two decades of OH variability as inferred by an inversion of atmospheric transport and chemistry of methyl chloroform, Atmos. Chem. Phys., 5, 2635–2656, doi:10.5194/acp-5-2635-2005, 2005.

ACPD

12, 30259–30282, 2012

Bruhwiler, L. M. P., Michalak, A. M., Peters, W., Baker, D. F., and Tans, P.: An improved Kalman Smoother for atmospheric inversions, Atmos. Chem. Phys., 5, 2691–2702, doi:10.5194/acp-5-2691-2005, 2005.

Denman, K. L., Brasseur, G., Chidthaisong, A., Ciais, P., Cox, P. M., Dickinson, R. E., Hauglustaine, D., Heinze, C., Holland, E., Jacob, D., Lohmann, U., Ramachandran, S., da Silva Dias, P. L., Wofsy, S. C., and Zhang, X.: Couplings between changes in the climate system and biogeochemistry, in: Climate Change 2007: The Physical Science Basis, Contribution of Working Group I to the Fourth Assessment Report of the Intergovernmental Panel on Climate Change, edited by: Solomon, S., Qin, D., Manning, M., Chen, Z., Marquis, M., Averyt, K. B., Tignor, M., and Miller, H. L., Cambridge Univ. Press, Cambridge, UK, chap. 7, 501–587, 2007.

Dlugokencky, E. J., Masarie, K. A., Lang, P. M., Tans, P. P., Steele, L. P., and Nisbet, E. G.: A dramatic decrease in the growth rate of atmospheric methane in the Northern Hemisphere during 1992, Geophys. Res. Lett., 21, 45–48, doi:10.1029/94GL00606, 1994.

Dlugokencky, E. J., Dutton, E. G., Novelli, P. C., Tans, P. P., Masarie, K. A., Lantz, K. O., and Madronich, S.: Changes in CH_4 and CO growth rate after the eruption of Mt. Pinatubo and their link with changes in tropical tropospheric UV flux, Geophys. Res. Lett., 23, 2761–2764, doi:10.1029/96GL02638, 1996.

Dlugokencky, E. J., Masarie, K. A., Lang, P. M., and Tans, P. P.: Continuing decline in the growth rate of atmospheric methane burden, Nature, 393, 447–450, 1998.

Dlugokencky, E. J., Houweling, S., Bruhwiler, L., Masarie, K. A., Lang, P. M., Miller, J. B., and Tans, P. P.: Atmospheric methane levels off: temporary pause or a new steady-state?, Geophys. Res. Lett., 30, 1992, doi:10.1029/2003GL018126, 2003.

Dlugokencky, E. J., Bruhwiler, L., White, J. W. C., Emmons, L. K., Novelli, P. C., Montzka, S. A., Masarie, K. A., Lang, P. M., Crotwell, A. M., Miller, J. B., and Gatti, L. V.: Observational constraints on recent increases in the atmospheric CH_4 burden, Geophys. Res. Lett., 36, L18803, doi:10.1029/2009GL039780, 2009.

Etheridge, D. M., Pearman, G. I., and Fraser, P. J.: Changes in tropospheric methane between 1841 and 1978 from a high accumulation rate Antarctic ice core, Tellus, 44, 282–294, 1992.

Enting, I. G.: Inverse Problems in Atmospheric Constituent Transport, Cambridge University Press, UK, 165–167, 2002.

Forster, P., Ramaswamy, V., Artaxo, P., Berntsen, T., Betts, R., Fahey, D. W., Haywood, J., Lean, J., Lowe, D. C., Myhre, G., Nganga, J., Prinn, R., Raga, G., Schulz, M., and Van Dorland, R.:

ACPD

12, 30259–30282, 2012

Changes in atmospheric constituents and in radiative forcing, in: Climate Change 2007: The Physical Science Basis, Contribution of Working Group I to the Fourth Assessment Report of the Intergovernmental Panel on Climate Change, edited by: Solomon, S., Qin, D., Manning, M., Chen, Z., Marquis, M., Averyt, K. B., Tignor, M., and Miller, H. L., Cambridge Univ. Press, Cambridge, UK, chap. 2, 131–234, 2007.

Fung, I., John, J., Lerner, J., Matthews, E., Prather, M., Steele, L. P., and Fraser, P. J.: Three-dimensional model synthesis of the global methane cycle, J. Geophy. Res., 96, 13033–13065, 1991.

Gelb, A., Kasper, J. F., Nash, R. A., Price, C. F., and Sutherland, A. A.: Applied Optimal Estimation, MIT Press, Cambridge, MA, 1974.

GLOBALVIEW-CH4: Cooperative Atmospheric Data Integration Project – Methane, CD-ROM, NOAA ESRL, Boulder, Colorado, available at: ftp://ftp.cmdl.noaa.gov/ccg/ch4/GLOBALVIEW, (last access: 21 October 2011), 2009a.

GLOBALVIEW-CO: Cooperative Atmospheric Data Integration Project – Carbon Monoxide, CD-ROM, NOAA ESRL, Boulder, Colorado, available at: ftp://ftp.cmdl.noaa.gov/ccg/ch4/GLOBALVIEW, (last access: 21 October 2011), 2009b.

Hartley, D. and Prinn, R.: Feasibility of determining surface emissions of trace gases using an inverse method in a three-dimensional chemical transport model, J. Geophy. Res., 98, 5183–5197, 1993.

Khalil, M. A. K., Butenhoff, C. L., and Rasmussen, R. A.: Atmospheric methane: trends and cycles of sources and sinks, Environ. Sci. Technol., 41, 2131–2137, 2007.

Manning, M. R., Lowe, D. C., Moss, R. C., Bodeker, G. E., and Allan, W.: Short-term variations in the oxidizing power of the atmosphere, Nature, 436, 1001–1004, 2005.

Patra, P. K., Houweling, S., Krol, M., Bousquet, P., Belikov, D., Bergmann, D., Bian, H., Cameron-Smith, P., Chipperfield, M. P., Corbin, K., Fortems-Cheiney, A., Fraser, A., Gloor, E., Hess, P., Ito, A., Kawa, S. R., Law, R. M., Loh, Z., Maksyutov, S., Meng, L., Palmer, P. I., Prinn, R. G., Rigby, M., Saito, R., and Wilson, C.: TransCom model simulations of CH_4 and related species: linking transport, surface flux and chemical loss with CH_4 variability in the troposphere and lower stratosphere, Atmos. Chem. Phys., 11, 12813–12837, doi:10.5194/acp-11-12813-2011, 2011.

Prinn, R. G., Weiss, R. F., Fraser, P. J., Simmonds, P. G., Cunnold, D. M., Alyea, F. N., O'Doherty, S., Salameh, P., Miller, B. R., Huang, J., Wang, R. H. J., Hartley, D. E., Harth, C., Steele, L. P., Sturrock, G., Midgley, P. M., and McCulloch, A.: A history of chemically and

ACPD
12, 30259–30282, 2012

radiatively important gases in air deduced from ALE/GAGE/AGAGE, J. Geophys. Res., 105, 17751–17792, 2000.

Prinn, R. G., Huang, J., Weiss, R. F., Cunnold, D. M., Fraser, P. J., Simmonds, P. G., McCulloch, A., Harth, C., Salameh, P., O'Doherty, S., Wang, R. H. J., Porter, L., and Miller, B. R.: Evidence for substantial variations of atmospheric hydroxyl radicals in the past two decades, Science, 292, 1882–1888, 2001.

Prinn, R. G., Huang, J., Weiss, R. F., Cunnold, D. M., Fraser, P. J., Simmonds, P. G., McCulloch, A., Harth, C., Reimann, S., Salameh, P., O'Doherty, S., Wang, R. H. J., Porter, L., Miller, B. R., and Krummel, P. B.: Evidence for variability of atmospheric hydroxyl radicals over the past quarter century, Geophys. Res. Lett., 32, L07809, doi:10.1029/2004GL022228, 2005.

Rigby, M., Prinn, R. G., Fraser, P. J., Simmonds, P. G., Langenfelds, R. L., Huang, J., Cunnold, D. M., Steele, L. P., Krummel, P. B., Weiss, R. F., O'Doherty, S., Salameh, P. K., Wang, H. J., Harth, C. M., Muhle, J., and Porter, L. W.: Renewed growth of atmospheric methane, Geophys. Res. Lett. 35, L22805, doi:10.1029/2008GL036037, 2008.

Ringeval, B., Friedlingstein, P., Koven, C., Ciais, P., de Noblet-Ducoudré, N., Decharme, B., and Cadule, P.: Climate-CH_4 feedback from wetlands and its interaction with the climate-CO_2 feedback, Biogeosciences, 8, 2137–2157, doi:10.5194/bg-8-2137-2011, 2011.

Seinfeld, J., Goteti, G., and Wood, E. F.: Development of a 50-year high-resolution global dataset of meteorological forcings for land surface modeling, J. Climate, 19, 3088–3111, 2006.

Steele, L., Dlugokencky, E. J., Lang, P. M., Tans, P. P., Martin, R. C., and Masarie, K. A.: Slowing down of the global accumulation of atmospheric methane during the 1980s, Nature, 358, 313–316, 1992.

Taraborrelli, D., Lawrence, M. G., Crowley, J. N., Dillon, T. J., Gromov, S., Gross, C. B. M., Vereecken, L., and Lelieveld, J.: Hydroxyl radical buffered by isoprene oxidation over tropical forests, Nat. Geosci., 5, 190–193, 2012.

Thompson, A. M. and Cicerone, R. J.: Atmospheric CH_4, CO and OH from 1860 to 1985, Nature, 321, 148–150, 1986.

Walter, B. P. and Heimann, M.: A process-based, climate-sensitive model to derive methane emission from natural wetlands: application to five wetland sites, sensitivity to model parameters, and climate, Global Biogeochem. Cy., 14, 745–765, 2000.

ACPD
12, 30259–30282, 2012

Zhuang, Q., Melillo, J. M., Kicklighter, D. W., Prinn, R. G., McGuire, A. D., Steudler, P. A., Felzer, B. S., and Hu, S.: Methane fluxes between terrestrial ecosystems and the atmosphere at northern high latitudes during the past century: a retrospective analysis with a process-based biogeochemistry model, Global Biogeochem. Cy., 18, GB3010, doi:10.1029/2004GB002239, 2004.

ACPD
12, 30259–30282, 2012

Table 1. Distributions of sources and sinks of CH_4, CO and OH in Northern and Southern Hemispheres (%).

	CH_4			CO		OH
	Natural Emissions	Anthropogenic Emissions	Soil Uptake	VOC Oxidation	Surface Deposition	VOC Oxidation
NH	65	83	78	50	50	50
SH	35	17	22	50	50	50

* Natural CH_4 emissions are $\sim 35\,Tg\,yr^{-1}$, including termites, ocean and hydrate emissions (wetland emissions are not included). Anthropogenic CH_4 emissions are $\sim 350\,Tg\,yr^{-1}$, including energy, landfill, ruminants, rice agriculture and biomass burning emissions. Soil uptake of CH_4 is $\sim 10\,Tg\,yr^{-1}$. The production of CO from VOC oxidation is $\sim 430\,Tg\,yr^{-1}$. Surface deposition of CO is $\sim 290\,Tg\,yr^{-1}$. The production of OH from VOC oxidation is $\sim 980\,Tg\,yr^{-1}$ (assuming 30 % OH produced in this way).

ACPD
12, 30259–30282, 2012

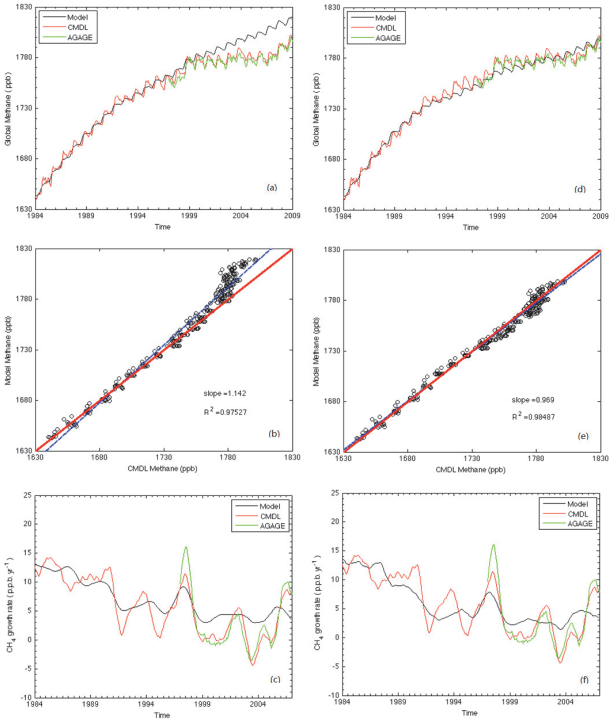

Fig. 1. The difference between observations and model simulations of global methane concentration (ppb) and methane growth rate (ppb yr^{-1}) in the recent decades. In **(a)**, **(b)** and **(c)**, simulation results (model) are from the changing OH scenario. In **(d)**, **(e)** and **(f)**, simulation results (model) are from the constant OH scenario. Two sets of observations are used here: GLOBALVIEW-CH4 data (CMDL) and AGAGE. In **(b)** and **(e)**, blue dashed lines are the linear regressions of the modeled methane concentrations against GLOBALVIEW-CH_4 measurements. The initial concentrations of CH_4, CO and OH are 1643 ppb, 93 ppb and 10^6 molecule cm^{-3}, respectively.

ACPD
12, 30259–30282, 2012

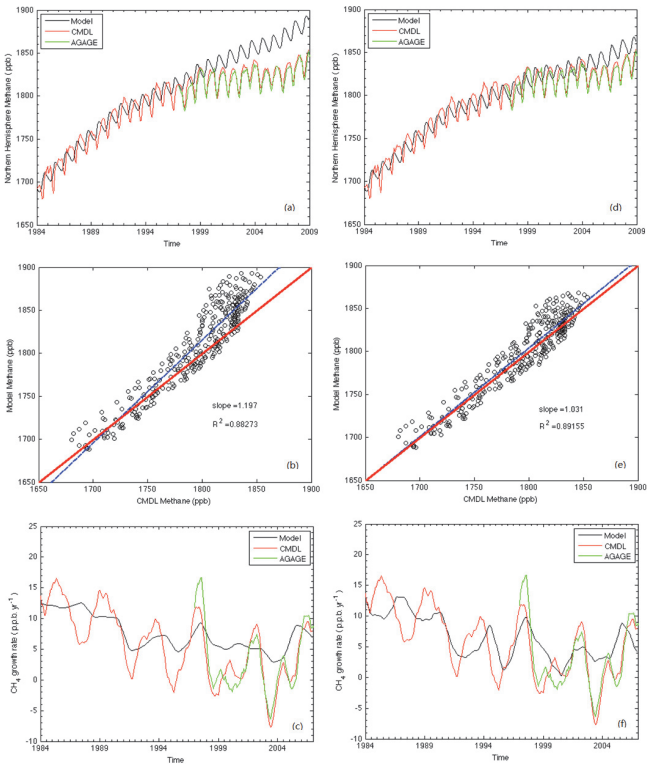

Fig. 2. The difference between observations and model simulations of NH methane concentration (ppb) and methane growth rate (ppb yr^{-1}) in the recent decades. In **(a)**, **(b)** and **(c)**, simulation results are from the changing OH scenario. In **(d)**, **(e)** and **(f)**, simulation results are from the constant OH scenario. In **(b)** and **(e)**, blue dashed lines are the linear regressions of the modeled methane concentrations against GLOBALVIEW-CH4 measurements. The initial concentrations of CH_4, CO and OH in NH are 1693 ppb, 120 ppb and 10^6 molecule cm^{-3}, respectively.

ACPD
12, 30259–30282, 2012

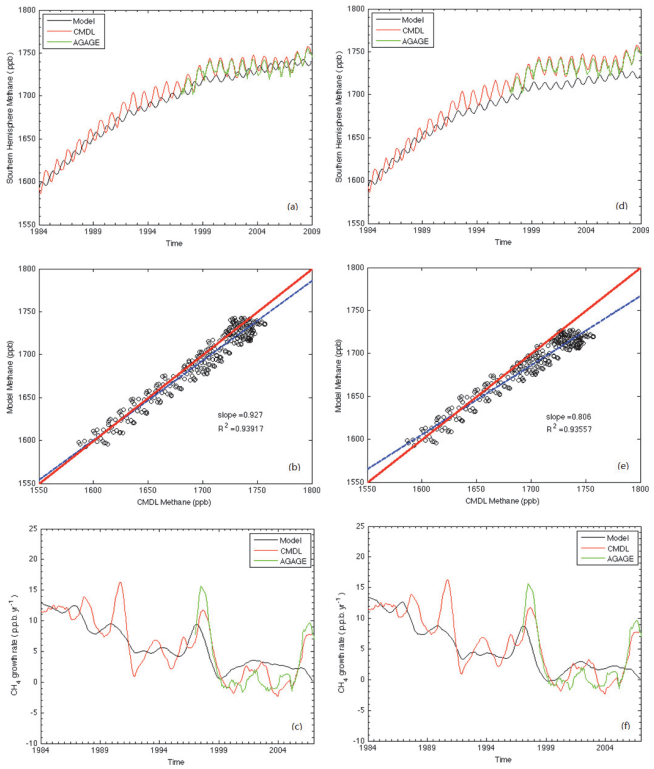

Fig. 3. The difference between observations and model simulations of SH methane concentration (ppb) and methane growth rate (ppb yr^{-1}) in the recent decades. In **(a)**, **(b)** and **(c)**, simulation results are from the changing OH scenario. In **(d)**, **(e)** and **(f)**, simulation results are from the constant OH scenario. In **(b)** and **(e)**, blue dashed lines are the linear regressions of the modeled methane concentrations against GLOBALVIEW-CH4 measurements. The initial concentrations of CH_4, CO and OH in SH are 1593 ppb, 66 ppb and 10^6 molecule cm^{-3}, respectively.

ACPD
12, 30259–30282, 2012

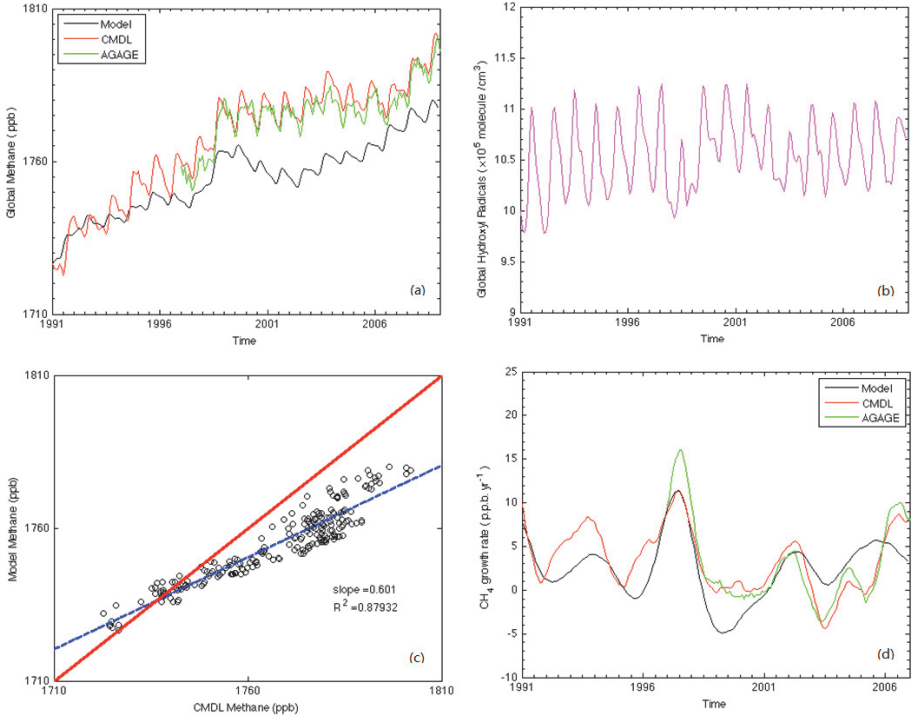

Fig. 4. The difference between observations and model simulations of global methane concentration (ppb) and methane growth rate (ppb yr^{-1}), and the trajectory of atmospheric OH concentration from 1991 to 2008. The concentrations of CO are given by GLOBALVIEW-CO data. The initial concentrations of CH_4 and OH are 1726.6 ppb and 10^6 molecule cm^{-3}, respectively.

ACPD
12, 30259–30282, 2012

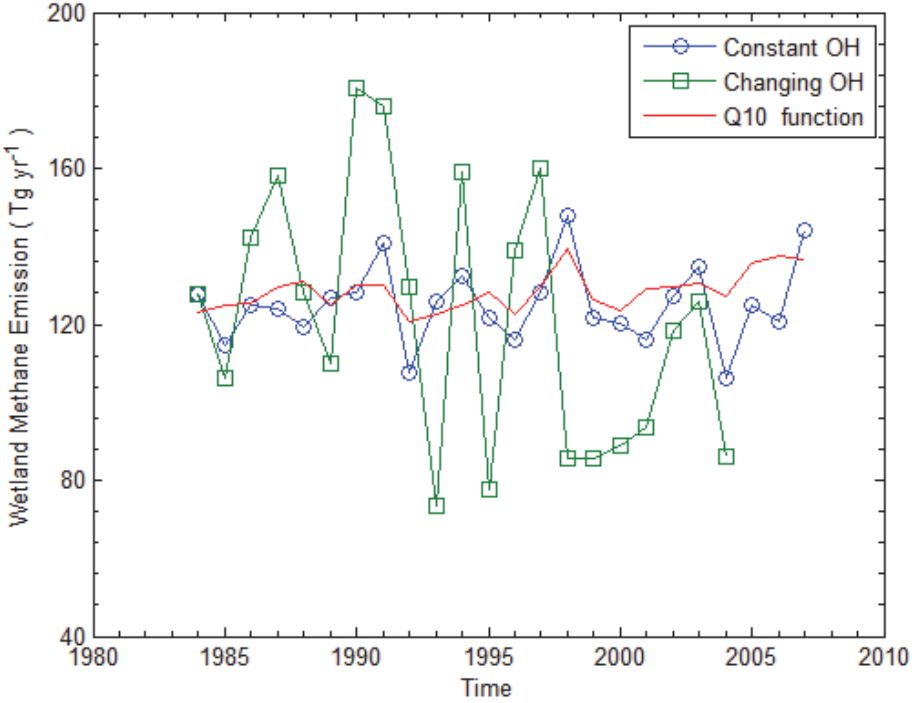

Fig. 5. The estimation of wetland methane emissions when assuming OH concentration is fixed at 10^6 molecule cm^{-3} (blue) and using changing OH concentrations (green), respectively. Red line is the values of Q_{10} function in Eq. (1).

ACPD
12, 30259–30282, 2012